Materials Today Communications 32 (2022) 104083

Contents lists available at ScienceDirect

Materials Today Communications

journal homepage: www.elsevier.com/locate/mtcomm

Study of optical and thermoelectric properties of double perovskites Cs_2KTlX_6 (X = Cl, Br, I) for solar cell and energy harvesting

Hind Albalawi [a], Ghulam M. Mustafa [b,*], Sadaf Saba [c], Nessrin A. Kattan [d], Q. Mahmood [e,f,**], H.H. Somaily [g,h], Manal Morsi [i,j], Sarah Alharthi [k], Mohammed A. Amin [k]

[a] Department of Physics, College of Sciences, Princess Nourah bint Abdulrahman University (PNU), P.O. Box 84428, Riyadh, 11671, Saudi Arabia
[b] Department of Physics, Division of Science and Technology, University of education, Lahore, Pakistan
[c] Centre of Excellence in Solid State Physics, University of the Punjab, Lahore, Pakistan
[d] Department of Physics, College of Science, Taibah University, Medina, Saudi Arabia
[e] Basic and Applied Scientific Research Center, Imam Abdulrahman Bin Faisal University, P. O. Box 1982, Dammam, 31441, Saudi Arabia
[f] Department of Physics, College of Science, Imam Abdulrahman Bin Faisal University, P. O. Box 1982, Dammam, 31441, Saudi Arabia
[g] Research Center for Advanced Materials Science (RCAMS), King Khalid University, Abha 61413, P.O. Box 9004, Saudi Arabia
[h] Department of Physics, Faculty of Science, King Khalid University, P.O. Box 9004, Abha, Saudi Arabia
[i] Department of Physics, College of Arts and Science, Wadi Addawasir, Prince Sattam bin Abdulaziz University, Kingdom of Saudi Arabia
[j] Department of Physics, Girl Collage for Art, Science, and Education, Ain-Shams University, Cairo, Egypt
[k] Department of Chemistry, College of Science, Taif University, P.O. Box 11099, Taif 21944, Saudi Arabia

ARTICLE INFO

Keywords:
Double perovskites
Spin-orbit coupling
Transport properties
Optical properties
Electronic properties

ABSTRACT

The double perovskites have emerging optical properties and extensively studied solar cells and renewable energy. In this work, we have investigated the optical, electronic and transport properties of Cs_2KTlX_6 (X = Cl, Br, I) using density functional theory. The thermodynamic stability is determined from the calculation of enthalpy of formation and structural stability is probed by computing the tolerance factor. Energy-volume optimization graphs reveal that lattice constant increased (11.31–12.80 Å) and bulk modulus decreased (20.46–15.90 GPa) with the increasing size of halogens. The optical properties are computed using TB-mBJ which reveals direct bandgaps (3.10, 2.0, 0.96) eV for (Cl, Br, I). In addition, the dielectric constant, refractive index, and reflectivity has been discussed in detail in the energy range of 0–6 eV. The absorption bands are recorded in infrared, visible and ultraviolet regions for Cl, Br and I based DPs. The temperature and chemical potential dependent transport properties are computed using BoltzTrap code. The appropriate values of thermoelectric parameters with high figure of merit at room temperature show the potential of these DPs for thermoelectric applications.

1. Introduction

Continuous increasing population put a high demand of energy consumption which is increasing tremendously with the passing years [1,2]. Renewable energy resources such as coal and gap are depleting rigorously, and these are supposed to be drained out till 2050. Therefore, there is an urgent need to look for alternative non-renewable and cost-effective energy resources [3,4]. Among these energy sources, solar and thermal energies are more reliable sources because solar cells and thermoelectric generators are portable devices and could be installed easily [5–7]. In this realm, one way is to increase the efficiencies of the existing optoelectronic and thermoelectric materials while other way is to discover new potential alternatives which is an integral part of this renewable energy research [8–12]. Therefore, an extensive research work is carried out to replace the Pb with some non-toxic metal to design the environment friendly halide based optoelectronic devices [13,14]. The materials suitable for optoelectronic devices must have high absorption coefficient, low reflectivity, and high optical conductivity [15,16]. Thus, Pb free halide-based perovskites (ABX_3) are suitable contestant but structural instabilities remained a big issue which motivated research community to explore new compositions [17].

Halide based double perovskites (DPs) with formula $ABB'X_6$ where *A*

* Corresponding author.
** Corresponding author at: Basic and Applied Scientific Research Center, Imam Abdulrahman Bin Faisal University, P. O. Box 1982, Dammam, 31441, Saudi Arabia.
E-mail addresses: gmmustafa25@gmail.com (G.M. Mustafa), qmmustafa@iau.edu.sa (Q. Mahmood).

https://doi.org/10.1016/j.mtcomm.2022.104083
Received 4 June 2022; Received in revised form 17 July 2022; Accepted 20 July 2022
Available online 22 July 2022

is an alkali metal, *B* and *B′* are transition or post transition metal and *X* is halide ion, received a considerable attention because of their novel features which emerge from merging of spin-orbit (SO) coupling, crystal field (CF) and Coulomb correlation [18,19]. For instance, transition metal (TM) based DPs exhibit exceptional characteristics including, suitable and tunable bandgap, highly stable structure, environment friendly nature, high charge mobility, half metallicity, thermoelectricity, superconductivity and piezoelectricity which are key features demanded for modern technological devices [20,21]. The proper working of any technological device is strongly influenced by the chemical nature of interface forming material in addition to its structural stability which make the study of defects present at the interface very crucial [22]. This is because the chemical composition of the interface plays a decisive role in controlling the electronic transportation at the interface [22].

Reports on the realization of wide spectrum applications of DPs, a significant work is devoted to exploring the potential of these compositions to meet the requirement of modern-day devices. For example, oxide-based DPs revealed extensive potential for advanced applications like La_2NiMnO_6, Bi_2NiMnO_6, Sr_2FeMoO_6 [23–26]. Igbari et al. comprehensively explored the photovoltaic aspects of double perovskites in their review article and highlighted the potential of DPs for futuristic optoelectronic devices [27–29]. Furthermore, Yan et al. experimentally synthesized the high-quality thin films of $Cs_2AgBiBr_6$ which behaved as a self-powered photodetector with 3 orders of magnitude increase in on-off ratio and favorable detectability [30,31]. Iqbal et al. investigated the optoelectronic properties of Rb_2AlInX_6 (X = Cl, Br, I) theoretically and checked their suitability for photovoltaic applications [32]. Hu et al. studied the structural, electronic, and optical properties of Cs_2TlAsX_6 using density functional theory and highlighted that bandgap value increased from 1.476 to 2.190 eV with decreasing ionic radius of halogen from iodine (I) to chlorine (Cl) [33]. Nawaz et al. studied the optoelectronic and thermoelectric characteristics of Rb_2YInX_6 (X = Cl, Br, I) for solar cell applications [34]. Over the past decade, scientific community focused on the thermoelectric response of DPs to check their appropriateness for thermoelectric generators. For instance, Aslam et al. inspected Cs_2InAgX_6 (X = Cl, Br, I) for futuristic photovoltaic devices [35]. The thallium element is toxic in its atomic form and rarely used for device applications. However, on compound formation its nature is changed and not remain harmful for applications. Moreover, there is lot of literature on double perovskites in which Tl has been used for optoelectronic and thermoelectric applications [36–38]. Here in this study, we have theoretically investigated the structural, optical, electronic and transport properties of Cs_2KTlX_6 (X = Cl, Br, I) and we believe that this study will provide solid basses for experimentalists working in this field.

2. Computational details

For theoretical investigation of different parameters of Cs_2KTlX_6 (X = Cl, Br, I), we implemented Wein2k code [39] based on DFT and employed linearized-augmented plane wave (LAPW) method [40]. First, the structure was generated and optimization using Birch-Murnaghan equation of states. This structural optimization was carried out PBE-GGA approximation by creating a k-mesh of 10 × 10 × 10 in which system picked 47 k-points for the calculations. For optical and thermoelectric properties, the kesh is make denser by taking the order 20×20×20. The product of muffin-tin radii and maximum K-vector $R_{MT} \times K_{max}$ was set to 8 while the value of G_{max} was kept as 16. The charge convergence criteria were set to 0.00001 Ry. To get the more reliable value of bandgap, the band structure was further optimized using TB-mBJ [41] because it improves the electronic band gap like experimental values. Lastly, the thermodynamic properties of these compositions were estimated using semiclassical Maxwell Boltzmann theory based BoltzTrap code. [42].

3. Results and discussion

3.1. Structural characteristics

The unit cell of Cs_2KTlX_6 (Cl/Br/I) compositions is represented in Fig. 1 which is a face-centered cubic structure with space group Fm-3 m [43,44]. In this unit cell the positions of Cs, K, Tl and X atoms is (0.25, 0.25, 0.25), (0, 0, 0), (0.5, 0.5, 0.5) and (x, 0, 0), respectively [43,45]. In this unit cell, the yellow-colored atoms, purple-colored atoms, ring-colored atoms and green-colored atoms correspond to Cs, K, Tl and X atoms, respectively.

The GGA-PBEsol was employed to explore the ground state structural parameters of the studied compositions. The computed lattice parameters a_o (Å) and bulk moduli B_o (GPa) of Cs_2KTlCl_6, Cs_2KTlBr_6 and Cs_2KTlI_6 are given in Table 1. The values of a_o (Å) increased from 11.31 Å to 12.05 Å and 12.80 Å and values of B_o (GPa) decreased from 20.46 GPa to 18.18 GPa and 15.90 GPa when Cl is replaced with Br and I [46]. To further examine thermodynamic stability formation energy has been computed by the chemical equation as [47].

$$H_f = E_{(Cs_aK_bTl_cX_d)} - (aE_{cs} + bE_K + cE_{Tl} + dE_X) \quad (1)$$

Here $E_{(Cs_aK_bTl_cX_d)}$, E_{cs}, E_K, E_{Tl}, and E_X are energies of Cs_2KTlX_6, Cs, K, Tl, and X atoms, respectively. The constants (a, b, c, d) are the number of elements in the balanced chemical equations. We have computed the energy of individual elements (Cs, K, Tl X) and the compounds Cs_2KTlX_6. The difference of energy has been measured as formation energy (H_f) as presented in Table 1. A decrease from − 2.33 to − 2.30 and − 2.23 was observed in the values of ΔH for Cs_2KTlCl_6, Cs_2KTlBr_6 and Cs_2KTlI_6 compositions, respectively. The endothermic phase decomposition confirmed the structural stability of all these compositions as represented by the negative values of ΔH. Goldsmith tolerance factor is a key parameter which determine the structural stability of perovskites. The stable structures must have the value of tolerance factor (t_f) in between 0.81 and 1.11 [48,49]. For present study, the values of t_f was 0.94, 0.92 and 0.87 for Cs_2KTlCl_6, Cs_2KTlBr_6 and Cs_2KTlI_6, respectively and provided in Table 1.

3.2. Electronic characteristics

The materials can be differentiated as metal, semiconductors or insulators on the basis of their bandgap values, carrier concentration and carrier mobilities. Hence, the electronic characteristics including band

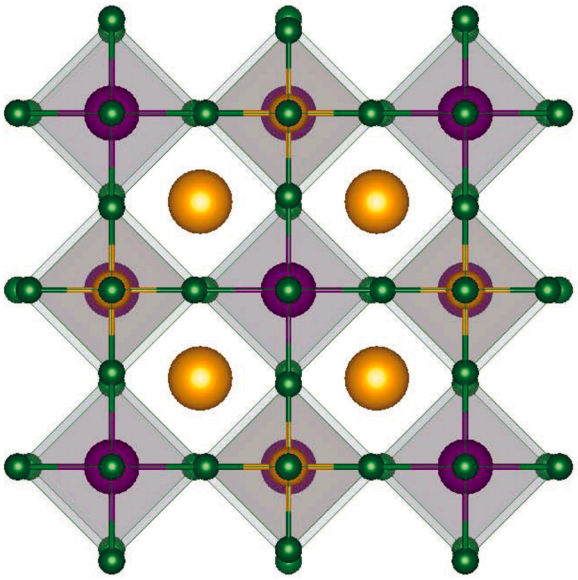

Fig. 1. Crystal structure of Cs_2KTlX_6 (X = Cl, Br, I) DPs in polyhedral form.

Table1
Structural and optical parameters of Cs_2KTlX_6 (X = Cl, Br, I).

Property	Cs_2KTlCl_6	Cs_2KTlBr_6	Cs_2KTlI_6
Lattice constant a_o (Å)	11.31	12.05	12.80
Bulk modulus B_o (*GPa*)	20.46	18.18	15.90
Enthalpy of formation H_f (eV)	-2.33	-2.30	-2.23
tolerance factor t_f	0.94	0.92	0.87
Band gap E_g(eV)	3.10	2.0	0.96
Static dielectric constant $\varepsilon_1(0)$	2.59	3.0	3.37
Static refractive index $n(0)$	1.61	1.74	1.93
Reflectivity R *(0)*	0.054	0.072	0.101

structure of materials under consideration are examined to check their nature either they are metallic or semiconductors so that their applications can be specified in various places. Fig. 2 (a-c) shows the band structure of these three compositions. These results are accurately computed using the TB-mBJ potential. The famous property of halide-based perovskites is their tunability of bandgap as their bandgap is reduced with the increase in radius of the halide ions [50]. From Fig. 2 (a-c), it is noticed that the top of valence bands and bottom of conduction bands of all three compositions appeared at same Γ-point so they have direct band gaps showing their semiconducting nature [45]. The replacement of Cl with Br and I in Cs_2KTlCl_6 composition caused a decrease in bandgap energy E_g(eV). The measured values of bandgap energies for composition Cs_2KTlX_6 were 3.10, 2.0 and 0.96 eV, respectively.

The density of states plots provide better insight of contributing states in band formation. The plot of PDOS of Cs_2KTlCl_6, Cs_2KTlBr_6, and Cs_2KTlI_6 DPs are shown in Fig. 3 (a-c). These graphs show that s states of Cs and K and p states of Tl and X are responsible for valence and conduction band formation. The edges of both bands are decorated by the p states of X. The position of p states in the valence band is fixed i.e. at the fermi level, while p state in the conduction band moves down towards fermi level as the ionic radius of the halogen atom increases. This movement of p-state in the conduction band is responsible for the reduction of bandgap. The bandgap values of Cs_2KTlCl_6 are found to be 3.10 eV which decreased to 2.0 and 0.96 eV when Cl is replaced by Br and I in the compositions [50]. Thus, substitution of halogens in the double perovskites is a sophisticated approach for their bandgap engineering which is required for their potential application for futuristic devices.

3.3. Optical characteristics

Sensitivity of any material towards light and its ability to convert it into electrical energy make it crucial for optoelectronic devices [51].

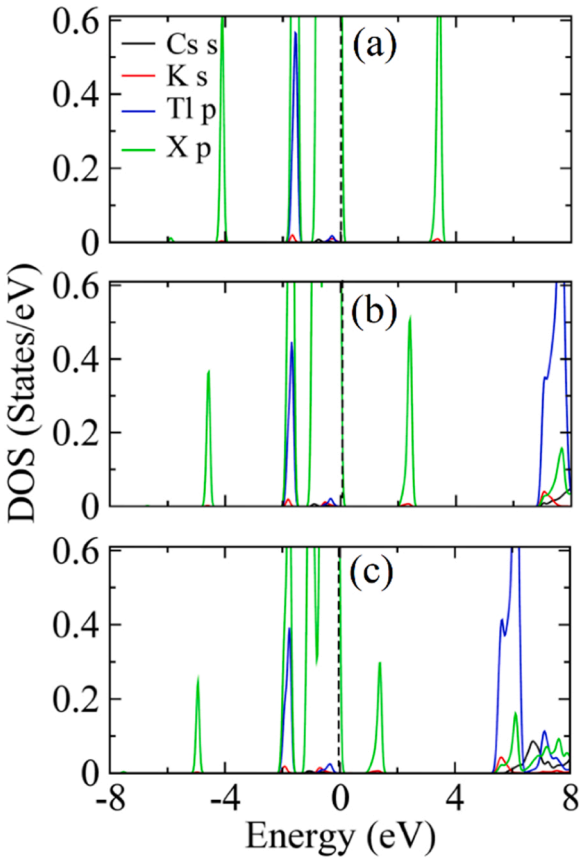

Fig. 3. density of states of (a) Cs_2KTlCl_6, (b) Cs_2KTlBr_6, and (c) Cs_2KTlI_6.

When light falls on semiconductor material having suitable bandgap, it generates electron hole pairs which when recombine gives electrical energy which could be utilized to perform multiple tasks. Fig. 4 (a) represents the plots of real part of dielectric constant ε_1 (ω), imaginary part of dielectric constant ε_2 (ω), refractive index n (ω) and absorption coefficient α (ω) in the energy range of 0–6 eV. When light interacts with the medium, it polarizes the medium which is quantified by the value of ε_1 while the energy losses due to dispersion of light are measured by the value of ε_2 (ω) [52]. The value of $\varepsilon_1(\omega)$ at 0 eV is called static dielectric constant ε(0). The measured values of ε(0) are given in Table1 as 2.59, 3.0 and 3.37 for Cs_2KTlCl_6, Cs_2KTlBr_6 and Cs_2KTlI_6, respectively. The value of $\varepsilon_1(\omega)$ increased with increasing energy of the incident light and

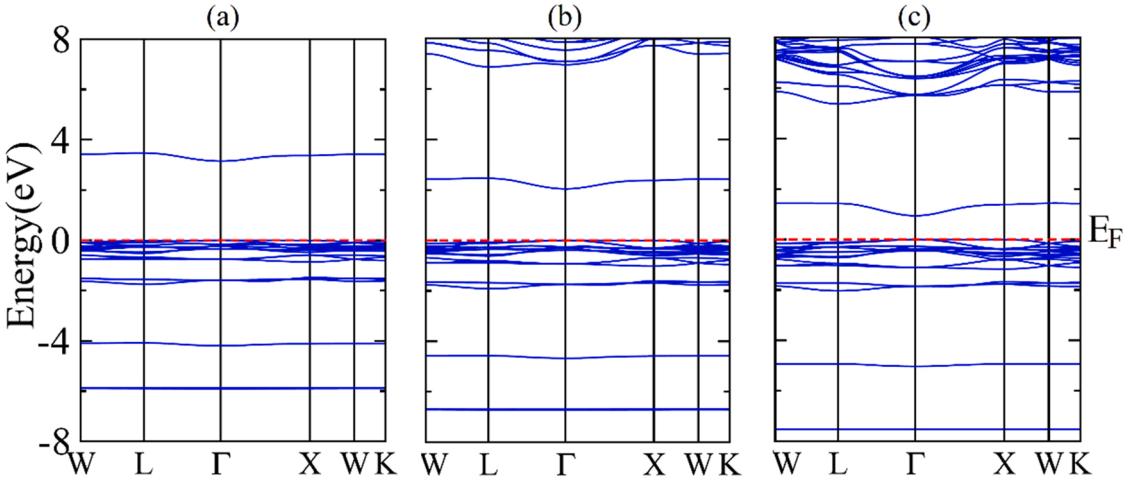

Fig. 2. Electronic band structures of (a) Cs_2KTlCl_6, (b) Cs_2KTlBr_6 and (c) Cs_2KTlI_6.

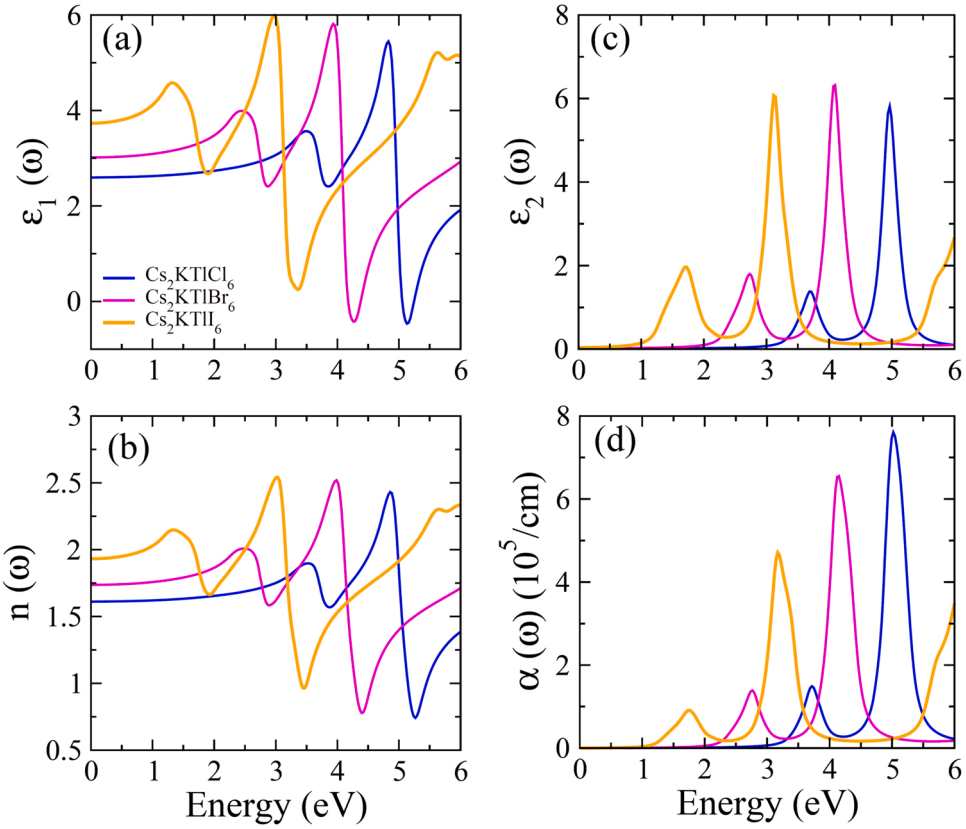

Fig. 4. (a) $\varepsilon_1(\omega)$ (b) n (ω), (c) ε_2 (ω) and (d) α (ω) of Cs_2KTlX_6 (X = Cl, Br, I).

show the peaks which are called relaxation peaks. From the position of these peaks, we can calculate the relaxation frequency or relaxation time [53]. The static value of ε_1 (ω) increased with increasing size of halogen which is attributed to the increasing polarizability of larger halogens. In addition, the position of relaxation peaks is shifted towards lower energy which is because relaxation frequency is inversely proportional to the net mass of oscillating atom [54]. The numerical value of refractive index n (ω) in the optical frequency range is determined by taking the

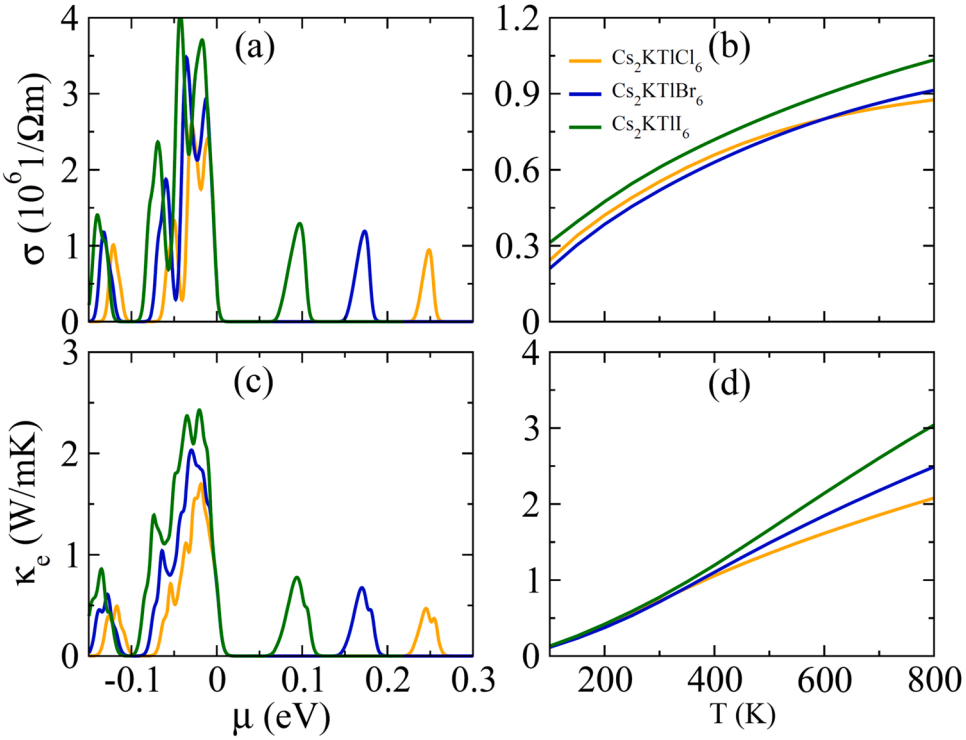

Fig. 5. (a, b) electrical conductivity (σ) and (c, d) thermal conductivity (κ_e) versus μ and T of Cs_2KTlX_6 (X = Cl, Br, I).

square root of ε_1 (ω). This is the reason why *n* shows the identical behavior as that of ε_1 (ω) with small values. The computed values of n (ω) for Cs_2KTlCl_6, Cs_2KTlBr_6 and Cs_2KTlI_6 are 1.61, 1.74 and 1.93, respectively. The variation of n (ω) with energy is shown in Fig. 4(b) while the variation of ε_2 (ω) against energy is shown in Fig. 4(c). The peaks appear in these graphs quantifies the energy loss because of interaction of light with materials. Fig. 4(d) represents the graph of absorption coefficient α (ω) in the energy range 0–6 eV. It shows the identical trend as that of ε_2 (ω) which indicates that the peaks in graph ε_2 (ω) correspond to the energy loss caused by the absorption of the material [55]. The absorption of light started at 3 eV energy for Cs_2KTlCl_6, at 2 eV for Cs_2KTlBr_6 and then at 1 eV for Cs_2KTlI_6.

3.4. Thermal characteristics

The material capable to change waste heat into electrical energy are termed as thermoelectric material and is potential candidate for energy harvesting technology [56]. The efficiency of thermoelectric material is computed in terms of dimensionless quantity called figure of merit that depends upon the electrical (σ) and thermal (κ) conductivities, Seebeck coefficient (S) and Power factor (PF). A suitable thermoelectric material is supposed to have higher values of all these parameters except thermal conductivity [57]. Usually, the ratio of electrical to thermal conductivity is 10^6 at any given temperature [58]. The Fig. 5 (a, b) represent the variation of σ versus chemical potential (μ) and temperature (T). The chemical potential quantifies the energy needed to add an electron in the system to overcome the repulsion of the system. It could have positive and negative values for n-type and p-type semiconductors [59]. In the given window of the chemical potential, the σ increased with increase in size of the halogens which is attributed to loosely bound and readily available valence electrons of halogens. An increasing trend in σ with temperature is observed. Since, the value of σ depends on the availability of the free carriers so the increasing conductivity with temperature indicates the increase in carrier concentration [60]. This carrier concentration increases due to the thermally broken bonds. The value of κ shows almost similar trend as that of the σ as shown in Fig. 5(c, d). The shifting of peaks towards lower μ may be due to the reduction in their bandgap values. The thermally generated charge carriers are responsible for the thermal conductivity [61]. The increase in the value of κ with temperature reflects that thermally generated charge carriers are increased.

The temperature gradient within the material defines the direction for electronic transportation. The temperature gradient of potential is termed as Seebeck coefficient (S) and play a determinantal role in probing the thermoelectric performance of the material. The variations of S and PF with respect to μ and temperature T are given in Fig. 6 (a, b). For good thermoelectric materials, the value of S should be around 200 μV/K [62]. These is a slight change in S for p-type region and a significant saw tooth variation in the n-type region. The value of S varies from 3.2 mV/K to − 3.2 mV/K which reflect the fact that majority charge carriers' switches from electrons to holes. In present study, the value of S was around 200 μV/K which decreased with increasing T and shows that increasing temperature reduced the concentration gradient and tries to make distribution of charge carrier's uniform. In addition, this variation may be due to the change in band structure or increase in electrical conductivity of the material.

Usually the thermoelectric performance of any material is judged by two different parameters which are power factor (PF) and figure of merit (ZT). PF determines the performance of the material by the combined effect of S and σ without considering the κ, whereas ZT also includes the thermal part of the conduction. The change of PF with μ and T are shown in Fig. 6 (c, d). The highest peaks of PF appeared in the negative value of μ which may be due to the presence of charge carriers [63]. When it is plotted versus T, it exposed almost same value at 0 K for all compositions which increased with T. The maximum increase in PF at higher T is observed for I based composition which may be due to the presence of larger number of charge carriers due to larger atomic number.

The T and μ dependent ZT is presented in Fig. 7(a, b). The peaks of ZT in the provided range of μ approaches unity which highlighted the importance of these material for thermoelectric device applications [64]. The value of ZT is decreased with increasing T value and noticed as 0.6 at RT for Cl based compositions and increased to 0.8 when Cl is

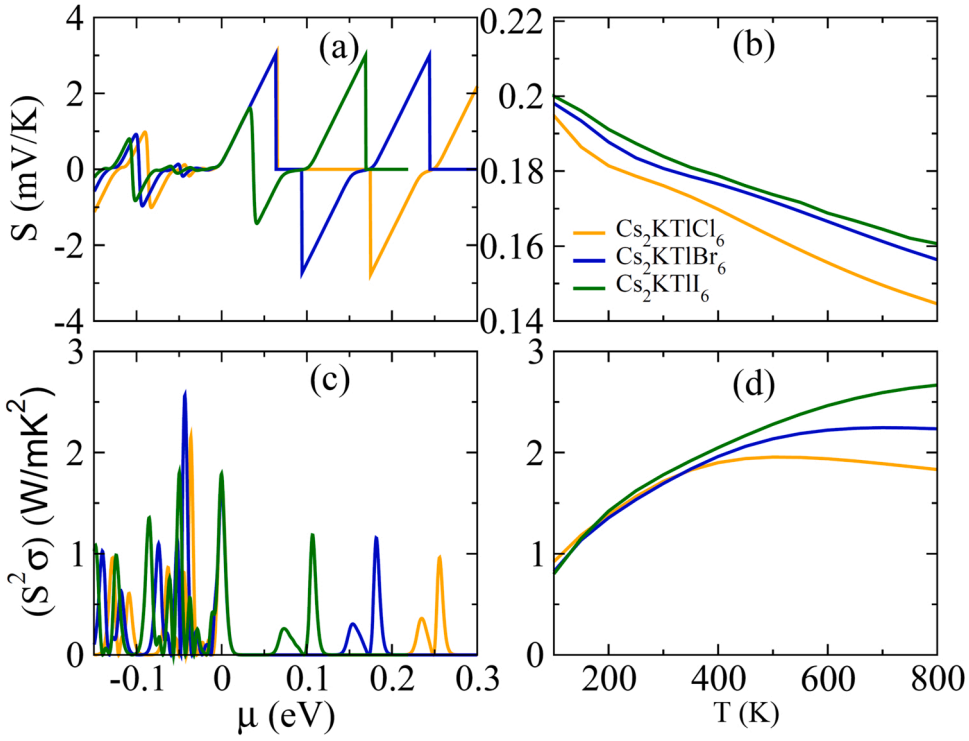

Fig. 6. (a, b) Seebeck coefficient (S), and Power factor ($S^2\sigma$) versus μ and T of Cs_2KTlX_6 (X = Cl, Br, I).

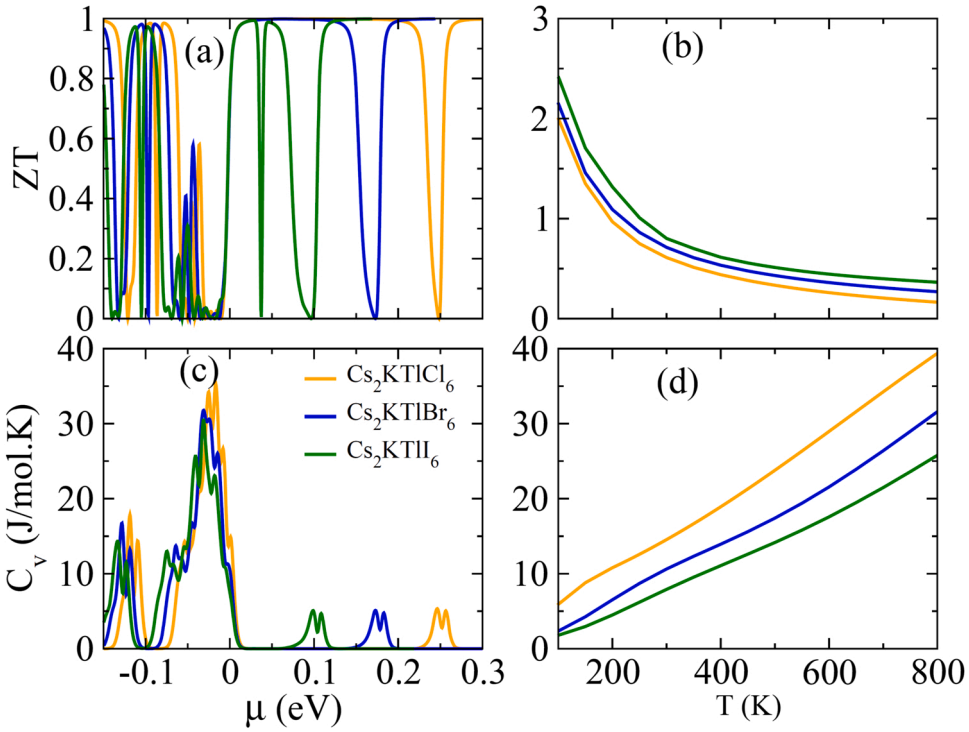

Fig. 7. (a, b) figure of merit (ZT), and (c, d) Specific heat capacity (Cv) versus μ and T of Cs_2KTlX_6 (X = Cl, Br, I).

replaced with Br and I which highlighted the suitability of these compositions for TE applications. The contribution of phonons in thermal conductivity can be estimated from the computed values of specific heat capacity (C_V) [65]. The computed values of C_V against μ and T are plotted in Fig. 7(c, d). The maximum peaks are shown in negative value of μ. The peaks appeared in positive μ range shifts towards 0 when larger halogens are placed in these DPs. The value of C_V increased linearly with increasing T and with the provided T range it did not get saturated. Most of the solids reach their saturation value when temperature exceeds Debye temperature.

4. Conclusion

In summary, we have computed the optical and transport properties of Cs_2KTlX_6 (X = Cl, Br, I) using DFT based Wien2k software. The thermodynamic and structural stabilities of these DPs were evaluated by computing the negative enthalpy of formation (−2.33 to −2.23 eV) and Goldsmith tolerance factor (0.94–0.87). The band structure revealed the significant contribution of *p*-states of halogens and Tl atoms in shaping the edges of valence and conduction bands. The movement of this *p*-state in conduction band towards fermi level on substitution of Cl with Br and I decrease the bandgap from 3.10 to 0.96 eV which make them diverse materials for optoelectronics from infrared to ultraviolet regions. The maximum absorption in visible range for Cs_2KTlBr_6 makes it potential material for solar cells. However, the static values of dielectric constant and refractive index increased from 2.59 to 3.37 and 1.61–1.93, respectively. The large values of figure of merit in temperature low temperature range and at 300 K increase their potential for thermoelectric generators.

CRediT authorship contribution statement

I, Dr. Qasim Mahmood declared that all the authors have been contributed equally. No part of the paper has been submitted to any and I will not submit it until the final decision from Materials Today Communication. We have not any conflict of interest.

Declaration of Competing Interest

The authors declare that they have no known competing financial interests or personal relationships that could have appeared to influence the work reported in this paper.

Data availability

Data will be made available on request.

Acknowledgment

This research was funded by Princess Nourah bint Abdulrahman University Researchers Supporting Project number (PNURSP2022R29), Princess Nourah bint Abdulrahman University, Riyadh, Saudi Arabia. The authors would like to thank Taif University Researchers Supporting Project number (TURSP-2020/200), Taif University, Taif, Saudi Arabia for supporting this project. This work was supported by King Khalid University through a grant (KKU/RCAMS/22) under the Research Center for Advanced Materials Science (RCAMS) at King Khalid University, Saudi Arabia.

References

[1] T.I. Al-Muhimeed, A. Shafique, A.A. AlObaid, M. Morsi, G. Nazir, M.M. AL-Anazy, Q. Mahmood, New lead-free double perovskites X_2GeI_6 (X= K, Rb, Cs) for solar cells, and renewable energy as an alternate of hybrid perovskites, Int. J. Energy Res. 45 (13) (2021) 19645–19652.

[2] Q. Mahmood, M. Younas, M.G.B. Ashiq, S.M. Ramay, A. Mahmood, H.M. Ghaithan, First principle study of lead-free double perovskites halides Rb2Pd (Cl/Br) 6 for solar cells and renewable energy devices: A quantum DFT, Int. J. Energy Res. 45 (10) (2021) 14995–15004.

[3] C.M. Vivek, P. Ramkumar, P.K. Srividhya, M. Sivasubramanian, Recent strategies and trends in implanting of renewable energy sources for sustainability–A review, Mater. Today.: Proc. 46 (2021) 8204–8208.

[4] M. Elangovan, Study of Solar Energy and Future Needs, Int. Res. J. Adv. Sci. Hub. 3 (2021) 23–28.

[5] S. Shoeibi, H. Kargarsharifabad, S.A.A. Mirjalily, M. Sadi, A. Arabkoohsar, A comprehensive review of nano-enhanced phase change materials on solar energy applications, J. Energy Storage 50 (2022), 104262.

[6] S. Shoeibi, H. Kargarsharifabad, M. Sadi, A. Arabkoohsar, S.A.A. Mirjalily, A review on using thermoelectric cooling, heating, and electricity generators in solar energy applications, Sustain. Energy Technol. Assess. 52 (2022), 102105.

[7] D. Sharma, R. Mehra, B. Raj, Comparative analysis of photovoltaic technologies for high efficiency solar cell design, Superlattices Microstruct. 153 (2021), 106861.

[8] X. Ma, Z. Li, J. Yang, Efficient direct band gap photovoltaic material predicted via doping double perovskites Cs2AgBiX6 (X= Cl, Br), J. Phys. Chem. C. 125 (20) (2021) 10868–10875.

[9] S.A. Moiz, A.N.M. Alahmadi, A.J. Aljohani, Design of a novel lead-free perovskite solar cell for 17.83% efficiency, IEEE Access 9 (2021) 54254–54263.

[10] T.H. Flemban, V. Singaravelu, A.A.S. Devi, I.S. Roqan, Homogeneous vertical ZnO nanorod arrays with high conductivity on an in situ Gd nanolayer, RSC Adv. 5 (115) (2015) 94670–94678.

[11] I.A. Ajia, P.R. Edwards, Z. Liu, J.C. Yan, R.W. Martin, I.S. Roqan, Excitonic localization in AlN-rich $Al_xGa_{1-x}N/AlyGa_{1-y}N$ multi-quantum-well grain boundaries, Appl. Phys. Lett. 105 (12) (2014), 122111.

[12] S. Maranghi, M.L. Parisi, R. Basosi, A. Sinicropi, The critical issue of using lead for sustainable massive production of perovskite solar cells: a review of relevant literature, Open Res. Eur. 1 (44) (2021) 44.

[13] N. Soleimanioun, M. Rani, B. Singh, G.S.S. Saini, S.K. Tripathi, Potential replacement to lead: Alkali metal potassium and transition metal zinc in organo-metal halide perovskite materials, J. Alloy. Compd. 861 (2021), 158207.

[14] F. Heidari Gourji, D. Velauthapillai, A Review on Cs-Based Pb-Free Double Halide Perovskites: From Theoretical and Experimental Studies to Doping and Applications, Molecules 26 (7) (2021) 2010.

[15] A.A. Ramanathan, J.M. Khalifeh, Electronic, magnetic, and optical properties of XScO3 (X= Mo, W) perovskites, PeerJ Mater. Sci. 3 (2021), e15.

[16] Z. Haman, M. Kibbou, I. Bouziani, Y. Benhouria, I. Essaoudi, A. Ainane, R. Ahuja, Structural, electronic, and optical properties of two-dimensional Janus transition metal oxides MXO (M= Ti, Hf and Zr; X= S and Se) for photovoltaic and opto-electronic applications, Phys. B: Condens. Matter 604 (2021), 412621.

[17] F. Bella, P. Renzi, C. Cavallo, C. Gerbaldi, Cesium for perovskite solar cells: an overview, Chem. Eur. J. 24 (47) (2018) 12183–12205.

[18] F. Igbari, Z.K. Wang, L.S. Liao, Progress of lead-free halide double perovskites, Adv. Energy Mater. 9 (12) (2019), 1803150.

[19] C. Martins, M. Aichhorn, S. Biermann, Coulomb correlations in 4d and 5d oxides from first principles—or how spin–orbit materials choose their effective orbital degeneracies, J. Phys.: Condens. Matter 29 (26) (2017), 263001.

[20] D. Sen, T. Saha-Dasgupta, Rational design of magnetic hybrid transition metal double perovskites in polyatomic anionic systems, Chem. Mater. 34 (4) (2022) 1821–1828.

[21] P. R Varadwaj, A2AgCrBr6 (A= K, Rb, Cs) and Cs2AgCrX6 (X= Cl, I) double perovskites: A transition-metal-based semiconducting material series with remarkable optics, Nanomaterials 10 (5) (2020) 973.

[22] Zhang, T., Hu, C., & Yang, S. (2020). Ion Migration: A "Double-Edged Sword" for Halide-Perovskite-Based Electronic Devices. Small Methods, 4(5), 1900552.

[23] P. Neenu Lekshmi, M. Raama Varma, Colossal Magneto-Dielectricity in La2NiMnO6 Probed by Raman Spectroscopy, in: In Materials Science Forum, Vol. 830, Trans Tech Publications Ltd,, 2015, pp. 513–517.

[24] A. Rathi, A. Anshul, A. Gupta, P.K. Rout, K.K. Maurya, R.K. Kotnala, G.A. Basheed, Large low-field magnetodielectric response in multiferroic Bi2NiMnO6 thin film, J. Phys. D: Appl. Phys. 50 (13) (2017), 135006.

[25] D. Yang, T. Yang, Q. Sun, Y. Chen, G.I. Lampronti, The annealing effects on the crystal structure, magnetism and microstructure of the ferromagnetic double perovskite Sr2FeMoO6 synthesized via spark plasma sintering, J. Alloy. Compd. 728 (2017) 337–342.

[26] K.I. Kobayashi, T. Kimura, Y. Tomioka, H. Sawada, K. Terakura, Y. Tokura, Intergrain tunneling magnetoresistance in polycrystals of the ordered double perovskite Sr 2 FeReO 6, Phys. Rev. B 59 (17) (1999) 11159.

[27] F. Igbari, Z.K. Wang, L.S. Liao, Progress of lead-free halide double perovskites, Adv. Energy Mater. 9 (12) (2019), 1803150.

[28] X. Liu, J. Fan, C. Huang, Advances in Theoretical Calculation of Halide Perovskites for Photocatalysis, Front. Nanotechnol. 3 (2021) 48.

[29] J. Luo, W. Zhang, H. Yang, Q. Fan, F. Xiong, S. Liu, B. Liu, Halide perovskite composites for photocatalysis: A mini review, EcoMat 3 (1) (2021), e12079.

[30] G. Yan, B. Jiang, Y. Xiao, C. Zhao, Y. Yuan, Z. Liang, Alkali metal ions induced high-quality all-inorganic Cs2AgBiBr6 perovskite films for flexible self-powered photodetectors, Appl. Surf. Sci. 579 (2022), 152198.

[31] A. Bibi, I. Lee, Y. Nah, O. Allam, H. Kim, L.N. Quan, D.H. Kim, Lead-free halide double perovskites: Toward stable and sustainable optoelectronic devices, Mater. Today 49 (2021) 123–144.

[32] S. Iqbal, G.M. Mustafa, M. Asghar, N.A. Noor, M.W. Iqbal, A. Mahmood, Y.H. Shin, Tuning the optoelectronic and thermoelectric characteristics of narrow bandgap Rb2AlInX6 (X= Cl, Br, I) double perovskites: A DFT study, Mater. Sci. Semicond. Process. 143 (2022), 106551.

[33] D.Y. Hu, X.H. Zhao, T.Y. Tang, L.M. Lu, L. Li, L.K. Gao, Y.L. Tang, Exploring the structural, electronic, and optical properties of vacancy-ordered double perovskites Cs2TlAsX6 (X= I, Br, Cl) based on first principles, Phys. Lett. A (2022), 127917.

[34] P.A. Nawaz, G.M. Mustafa, S.S. Iqbal, N.A. Noor, T.S. Ahmad, A. Mahmood, R. Neffati, Theoretical investigations of optoelectronic and transport properties of Rb2YInX6 (X= Cl, Br, I) double perovskite materials for solar cell applications, Sol. Energy 231 (2022) 586–592.

[35] F. Aslam, B. Sabir, M. Hassan, Structural, electronic, optical, thermoelectric, and transport properties of indium-based double perovskite halides Cs2InAgX6 (X= Cl, Br, I) for energy applications, Appl. Phys. A 127 (2) (2021) 1–12.

[36] H.H. Hegazy, G.M. Mustafa, A. Nawaz, N.A. Noor, A. Dahshan, I. Boukhris, Tuning of direct bandgap of Rb_2ScTlX_6 (X = Cl, Br, I) double perovskites through halide ion substitution for solar cell devices, J. Mater. Res. Technol. 19 (2022) 1271–1281.

[37] M. Manzoor, M.W. Iqbal, M. Imran, N.A. Noor, A. Mahmood, Y.M. Alanazi, S. Aftab, Probing direct bandgap of double perovskites Rb_2LiTlX_6 (X = Cl, Br) and optoelectronic characteristics for Solar cell applications: DFT calculations, J. Mater. Res. Technol. 18 (2022) 4775–4785.

[38] Q. Mahmood, G. Nazir, S. Bouzgarrou, A.I. Aljameel, A. Rehman, H. Albalawi, B. U. Haq, T. Ghrib, A. Mera, Study of new lead-free double perovskites halides Tl_2TiX_6 (X = Cl, Br, I) for solar cells and renewable energy devices, J. Solid State Chem. 308 (2022), 122887.

[39] P. Blaha, K. Schwarz, G.K.H. Madsen, D. Kvasnicka, J. Luitz, WIEN2K, An Augmented Plane Wave + local Orbitals Program for Calculating Crystal Properties. Karl Heinz Schwarz, Techn, Universitat Wien,, Austria, 2001.

[40] P. Blaha, K. Schwarz, P. Sorantin, S.K. Trickey, Full-potential, linearized augmented plane wave programs for crystalline systems, Comput. Phys. Commun. 59 (1990) 339.

[41] F. Tran, P. Blaha, Accurate Band Gaps of Semiconductors and Insulators with a Semi-local Exchange-Correlation Potential, Phys. Rev. Lett. 102 (2009), 226401.

[42] G.K.H. Madsen, K. Schwarz, D.J. Singh, BoltzTraP. A code for calculating band-structure dependent quantities, Comput. Phys. Commun. 175 (2006) 67.

[43] G. Volonakis, A.A. Haghighirad, R.L. Milot, W.H. Sio, M.R. Filip, B. Wenger, M. B. Johnston, L.M. Herz, H.J. Snaith, F. Giustino, Cs2InAgCl6: a new lead-free halide double perovskite with direct band gap, J. Phys. Chem. Lett. 8 (4) (2017) 772–778.

[44] M.T. Anderson, K.B. Greenwood, G.A. Taylor, K.R. Poeppelmeier, B-cation arrangements in double perovskites, Prog. Solid State Chem. 22 (3) (1993) 197–233.

[45] E. Haque, M.A. Hossain, Electronic, phonon transport and thermoelectric properties of Cs2InAgCl6 from first-principles study, Comput. Condens. Matter 19 (2019), e00374.

[46] J. Luo, S. Li, H. Wu, Y. Zhou, Y. Li, J. Liu, J. Li, K. Li, F. Yi, G. Niu, J. Tang, Cs2AgInCl6 double perovskite single crystals: parity forbidden transitions and their application for sensitive and fast UV photodetectors, ACS Photon 5 (2) (2017) 398–405.

[47] N.H. Alotaibi, G.M. Mustafa, N.A. Kattan, Q. Mahmood, H. Albalawi, M. Morsi, H. H. Somaily, M.A.H. Hisham, I. Mahmoud, M.A. Amin, DFT study of double perovskites Cs_2AgBiX_6 (X = Cl, Br): An alternative of hybrid perovskites, J. Solid State Chem. 313 (2022), 123353.

[48] C.J. Bartel, C. Sutton, B.R. Goldsmith, R. Ouyang, C.B. Musgrave, L.M. Ghiringhelli, M. Scheffler, New tolerance factor to predict the stability of perovskite oxides and halides, Sci. Adv. 5 (2) (2019) eaav0693.

[49] A.E. Fedorovskiy, N.A. Drigo, M.K. Nazeeruddin, The role of Goldschmidt's tolerance factor in the formation of A2BX6 double halide perovskites and its optimal range, Small Methods 4 (5) (2020), 1900426.

[50] J.H. Noh, S.H. Im, J.H. Heo, T.N. Mandal, S.I. Seok, Chemical management for colorful, efficient, and stable inorganic–organic hybrid nanostructured solar cells, Nano Lett. 13 (4) (2013) 1764–1769.

[51] S. Wu, Z. Chen, H.L. Yip, A.K.Y. Jen, The evolution and future of metal halide perovskite-based optoelectronic devices, Matter 4 (12) (2021) 3814–3834.

[52] M. Faizan, K.C. Bhamu, G. Murtaza, X. He, N. Kulhari, M.M. AL-Anazy, S.H. Khan, Electronic and optical properties of vacancy ordered double perovskites A2BX6 (A= Rb, Cs; B= Sn, Pd, Pt; and X= Cl, Br, I): a first principles study, Sci. Rep. 11 (1) (2021) 1–9.

[53] A. Natik, Y. Abid, R. Moubah, M. Abid, H. Lassri, Ab-initio investigation of the structural, electronic, and optical properties of lead-free halide Cs_2TiI_6 double perovskites, Solid State Commun. 319 (2020), 114006.

[54] T. Atsue, I.B. Ogunniranye, O.E. Oyewande, Investigation of material properties of halide mixed lead-Free double perovskite for optoelectronic applications using first-principles study, Mater. Sci. Semicond. Process. 133 (2021), 105963.

[55] N.I. Ibrahim, F.A. Al-Sulaiman, F.N. Ani, Solar absorption systems with integrated absorption energy storage–A review, Renew. Sustain. Energy Rev. 82 (2018) 1602–1610.

[56] J. Wei, L. Yang, Z. Ma, P. Song, M. Zhang, J. Ma, X. Wang, Review of current high-ZT thermoelectric materials, J. Mater. Sci. 55 (27) (2020) 12642–12704.

[57] M.A. Ali, T. Alshahrani, G. Murtaza, Defective perovskites Cs2SeCl6 and Cs2TeCl6 as novel high temperature potential thermoelectric materials, Mater. Sci. Semicond. Process. 127 (2021), 105728.

[58] Lee, W., Li, H., Wong, A.B., Zhang, D., Lai, M., Yu, Y.,. & Yang, P. (2017). Ultralow thermal conductivity in all-inorganic halide perovskites. Proceedings of the National Academy of Sciences, 114(33), 8693–8697.

[59] G. Wu, X. Yu, Contributions of chemical potential to the diffusive Seebeck coefficient for bulk semiconductor materials, Eur. Phys. J. 135 (6) (2020) 1–15.

[60] M. Sajjad, Q. Mahmood, N. Singh, J.A. Larsson, Ultralow lattice thermal conductivity in double perovskite Cs2PtI6: a promising thermoelectric material, ACS Appl. Energy Mater. 3 (11) (2020) 11293–11299.

[61] T. Alshahrani, G.M. Mustafa, T.H. Flemban, H. Althib, S. Al-Qaisi, N.A. Kattan, Q. Mahmood, Probing of optoelectronic and transport properties of zinc based ZnY2×4 (X= S, Se) spinels for renewable energy, ECS J. Solid-State Sci. Technol. 9 (10) (2020), 105001.

[62] N.A. Noor, M. Rashid, G.M. Mustafa, M.I. Khan, A. Mahmood, S.M. Ramay, Study of pressure induced physical properties of ZnZrO3 perovskite using density functional theory, Chem. Phys. Lett. 753 (2020), 137601.

[63] J. Cao, D. Ekren, Y. Peng, F. Azough, I.A. Kinloch, R. Freer, Modulation of charge transport at grain boundaries in SrTiO3: toward a high thermoelectric power factor at room temperature, ACS Appl. Mater. Interfaces 13 (10) (2021) 11879–11890.
[64] H.J. Goldsmid, Improving the thermoelectric figure of merit, Sci. Technol. Adv. Mater. 22 (1) (2021) 280–284.
[65] Q. Mahmood, M. Hassan, T.H. Flemban, B.U. Haq, S. AlFaify, N.A. Kattan, A. Laref, Optoelectronic and thermoelectric properties of double perovskite Rb2PtX6 (X= Cl, Br) for energy harvesting: first-principles investigations, J. Phys. Chem. Solids 148 (2021), 109665.